A DISCRETE TOMOGRAPHY APPROACH FOR SUPERRESOLUTION MICRO-CT IMAGES: APPLICATION TO BONE

Gert Van Gompel, K. Joost Batenburg*, Elke Van de Casteele† , Wim Van Aarle*, Jan Sijbers**

*University of Antwerp, IBBT-Visionlab, Antwerp, Belgium
† SkyScan, Kontich, Belgium

ABSTRACT

In micro-CT imaging, the effective spatial resolution of the reconstructed images is generally limited by X-ray dose restrictions, the detector configuration or the scanning geometry. In this paper, we show that, using prior information on the grey values of the scanned objects, the spatial resolution of the reconstructed images can dramatically be improved. The proposed method is based on an upsampling of the reconstruction grid, combined with the DART algorithm (discrete algebraic reconstruction technique [1]), in which the scanned object is assumed to be composed of homogeneous materials. Experiments were run on simulated data as well as real X-ray CT data of the rat trabecular bone. Results show that the proposed method generates reconstructions with significantly more detail compared to conventional reconstruction algorithms.

Index Terms— CT, computed tomography, superresolution, discrete tomography, bone

1. INTRODUCTION

In numerous μCT applications, the path to qualitative high resolution images is obstructed by X-ray dose limitations, or scanning times [2]. Indeed, the use of a high resolution detector for reconstruction on a refined grid leads to a correspondingly decreased signal to noise ratio since a similar number of photons is subdivided over more detector pixels. Alternatively, zooming in on a specific region of interest in the object as to increase the resolution of that region, has the drawback of projection truncation, which leads to cupping artifacts in the resulting reconstructions.

In our approach, the aim is to reconstruct the image on an upsampled grid. Since this problem is highly underdetermined, prior knowledge is included to resolve the non-uniqueness of the solution. A variety of algorithms exists that exploit prior knowledge to compute an accurate reconstruction even if the underlying system of equations is underdetermined. One example is the discrete algebraic reconstruction technique

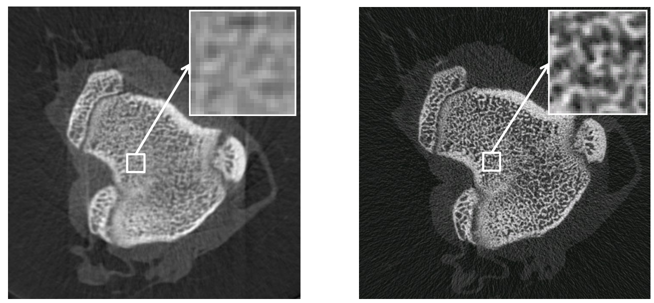

(a) 35μm pixel size (b) 9μm pixel size

Fig. 1. Reconstructions from real X-ray CT data of rat trabecular bone that was scanned at two different resolutions

(DART) [1], which is an iterative algorithm that assumes the object to be piecewise uniform with known densities. In this work, DART is applied for the reconstruction of piecewise constant objects on an upsampled grid. Note that the application of DART results in a segmented image. Indeed, DART finds the piecewise constant image that minimizes the projection distance (i.e. the difference between the measured data and the Radon transform of the reconstructed image). This is essentially different from finding the optimal segmentation of a continuous reconstruction from the dataset.

An important application in μCT imaging is the reconstruction of trabecular bone. In certain preclinical studies, the temporal effect of certain drugs on the bones of mice and rats is investigated by scanning the animals every few weeks. To prevent a change in bone structure due to X-ray exposure, the dose should remain as low as possible, which strikes off the option of scanning at higher resolutions with the same signal to noise ratio. Nevertheless, especially for small animal bone studies, it is very important that an adequate resolution is obtained for the visualization of the smallest trabecular structures and to enable a sufficiently accurate segmentation in order to accurately determine the morphometric bone parameters [3]. In Fig. 1 (a), an example of a realistic CT reconstruction of a rat bone slice is shown. It can be observed that segmentation from this image is a difficult task,

This work was financed by IWT Flanders (SBO-QUANTIVIAM). K. J. Batenburg also acknowledges the support of FWO, Flanders.

while the reconstruction of a similar slice in a high resolution scan of the bone (dose $\times 16$) (see Fig. 1(b)), is clearly easier to segment. In practice, one often empirically selects a global threshold, which remains fixed throughout a series of experiments for consistent analysis. In order to evaluate which trabecular thicknesses will be undetected in the segmented image, the user can perform a calibration scan with aluminium foils.

In this paper, the proposed discrete tomography technique for the reconstruction on an upsampled grid, is applied to simulated and real X-ray CT datasets of rat trabecular bone as to increase the effective spatial resolution of the reconstructions and to provide a segmented image.

This paper is organized as follows. Section 2 explains the theory behind our approach. Section 3 describes how the simulated data is computed. Experiments were run on simulated data as well as real X-ray CT data of the rat trabecular bone. The description of these experiments and the results are summarized in Section 4. Finally, conclusions are drawn in Section 5.

2. SUPERRESOLUTION BY DISCRETE TOMOGRAPHY

Consider a sinogram consisting of M projections with N radial samples at sampling distance $\Delta s = 1$. Such a dataset is typically reconstructed on an $N \times N$ grid, with sampling distance $\Delta t = \Delta s = 1$ (see Fig. 2(a)).
Algebraic methods consider reconstruction as the problem of solving a system of linear equations

$$\boldsymbol{A}\boldsymbol{x} = \boldsymbol{p} \tag{1}$$

where $\boldsymbol{x} = (x_j)$ are the unknown attenuation values on the grid in image domain, $\boldsymbol{p} = (p_i)$ are the measured projection values, and $\boldsymbol{A} = (a_{i,j})$ is the linear projection operator. Consider an ideal experiment, without noise, where a sufficient number of projections is available to ensure that the system in Eq. (1) has a unique solution. Now suppose that prior knowledge about the object is available. In case of bone, this prior knowledge could be the uniform density of the bone. The combination of the complete dataset and the prior knowledge represents an overdetermined reconstruction problem. Hence, parts of the projection data contain redundant information. To optimally exploit this redundant data, we transform the reconstruction problem on the $N \times N$ grid to a limited data reconstruction problem on an $aN \times aN$ grid with sampling distance $\Delta\tilde{t} = 1/a$ for some integer $a > 1$. Note that the sampling distance of the detector pixels is now larger than the sampling distance of the refined grid. Each detector pixel can be seen as the sum of contributions of a subdetector pixels with sampling distance $\Delta\tilde{s} = 1/a\Delta s = 1/a$ which corresponds to the sampling distance of the refined grid (see Fig. 2(b)). Compared to the system in Eq. (1), the system

$$\tilde{\boldsymbol{A}}\boldsymbol{y} = \boldsymbol{p} \tag{2}$$

corresponding to the upsampled reconstruction grid has the same number of equations, while the number of unknowns has increased by a factor a^2, resulting in an *underdetermined reconstruction problem*.

We now apply the DART algorithm for discrete tomography, which solves the system in Eq. (2) under the constraint that each of the y_i can only take values in a prescribed set $R = \{\rho_1, \ldots, \rho_k\}$. In the case of bone, this set of admissible grey levels will consist of three values, for the background, the soft tissue and bone, respectively. DART is an iterative heuristic algorithm that combines regular iterative reconstruction algorithms, such as ART or SIRT, with segmentation, boundary detection and constrained reconstruction steps. It has recently been applied successfully to limited data problems in electron tomography. We refer to [1] for more details. In the next section, we will demonstrate that by exploiting the discreteness in the grey level domain, DART can compute a solution of the system in Eq. (2) that accurately represents the scanned bone, even though the equation system is basically underdetermined.

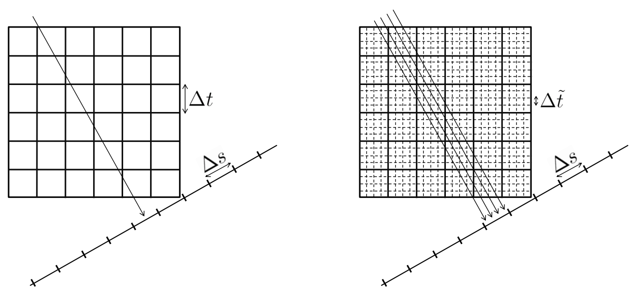

(a) (b)

Fig. 2. (a) reconstruction grid used for conventional CT. (b) reconstruction grid in the proposed discrete tomography approach

3. PHANTOM AND DATA SIMULATION

A dataset was simulated that incorporates following two basis assumptions:

- Bone has a uniform density
- Trabecular bone structures can be tiny, and consequently, partial volume problems take place, i.e. a pixel in the reconstruction grid may partially consist of bone and air.

Two bone slices (Fig. 3(a) and (b)) were simulated based on FBP reconstructions from real X-ray CT data of a rat femur, which was scanned at a 35μm resolution in a SkyScan 1076

(a) Phantom A (b) Phantom B

Fig. 3. Simulated phantoms of rat trabecular bone, with densities $R = \{0, 1\}$

scanner. The first phantom represents a bone slice near the growing plate, hence consists of very fine structures. The second phantom represents a slice through trabecular bone which is often investigated in bone studies. Both phantoms are binary (with gray values $0, 1$) and contain details of up to 1 pixel. A complete sinogram (1024×360) with 1024 radial samples and 360 angles between $\theta \in [0, \pi)$ is computed. The partial volume problem is simulated by downsampling each projection to 256 radial samples by summing the radial bins 4 by 4. The resulting sinogram is used for the reconstructions in the various experiments.

4. EXPERIMENTS AND RESULTS

Let $\boldsymbol{p} = (p_1, ..., p_i, ..., p_{N \times M})$ represent a 2D sinogram which consists of M projections with N radial samples. From this dataset, following reconstruction experiments are run:

(a) Standard FBP reconstruction on the $N \times N$ grid.

(b) DART reconstruction on the $N \times N$ grid.

(c) FBP reconstruction on a refined $aN \times aN$ grid (with $a = 8$) from an upsampled sinogram. The upsampling of the sinogram is performed in the radial direction by 1D linear interpolation such that each projection consists of aN pixels with pixel width $\Delta t = 1/a$ and $a > 1$ an integer.

(d) DART reconstruction on the refined $aN \times aN$ grid (with $a = 8$) from the original $N \times M$ sinogram according to the approach explained in Section 2.

To quantify the reconstruction quality, we compute the number of misclassified pixels (NMP) with respect to the ground truth images in Fig. 3. Since the experiments are performed at varying resolutions, the reconstructions first need to be rescaled to the size of the ground truth images. Images with a larger grid (2048×2048) than the ground truth image, are downsampled by averaging the pixel values in blocks of 2×2 pixels. If the reconstruction has a grid size smaller than 1024×1024, the image is upsampled using bilinear interpolation. After the resampling, all images are binarized using the threshold $t = 0.5$.

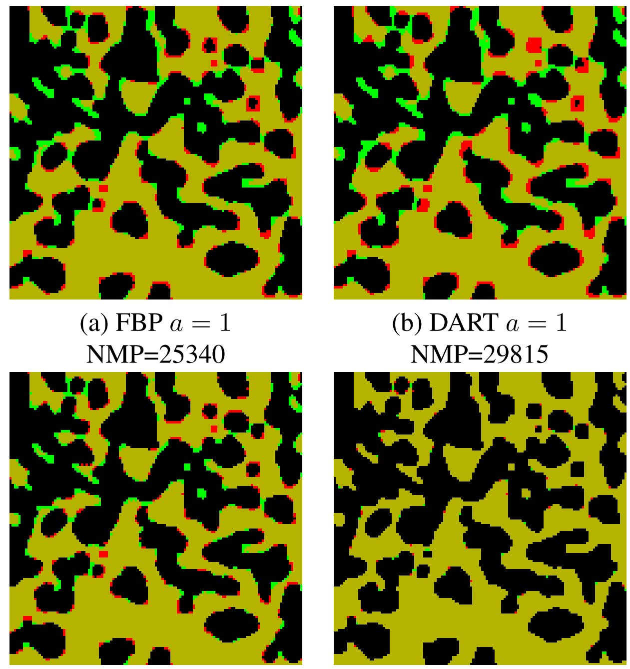

(a) FBP $a = 1$ NMP=25340
(b) DART $a = 1$ NMP=29815
(c) FBP $a = 8$ NMP=19085
(d) DART $a = 8$ NMP=1420

Fig. 4. Thresholded FBP and DART reconstructions of Phantom A, for different levels of grid upsampling, and from 360 projections with 256 radial samples.

Fig. 4 and 5 depict reconstructions of Phantom A from 360 projections and Phantom B from only 36 projections. The subfigures (a) to (d) in each of these figures correspond to the above mentioned reconstruction experiments (a) to (d). In each subfigure, the reconstruction is displayed in red and the ground truth image in green. Where both images overlap, the corresponding pixel is colored in yellow. Note in Fig. 4(b) that the DART reconstruction on an $N \times N$ grid does not necessarily improve the reconstruction accuracy compared to the FBP reconstruction for $a = 1$, which is due to the fact that DART intrinsically suffers from a small loss of spatial resolution. However, the small number of misclassified pixels (NMP) in the upsampled DART reconstruction demonstrates that even for very complex phantoms, a drastic improvement of the image accuracy can be obtained. Fig. 5(d) shows that it is even possible to obtain accurate reconstruction of the smallest trabecular structures on an upsampled grid, from a dataset with only 36 projections.

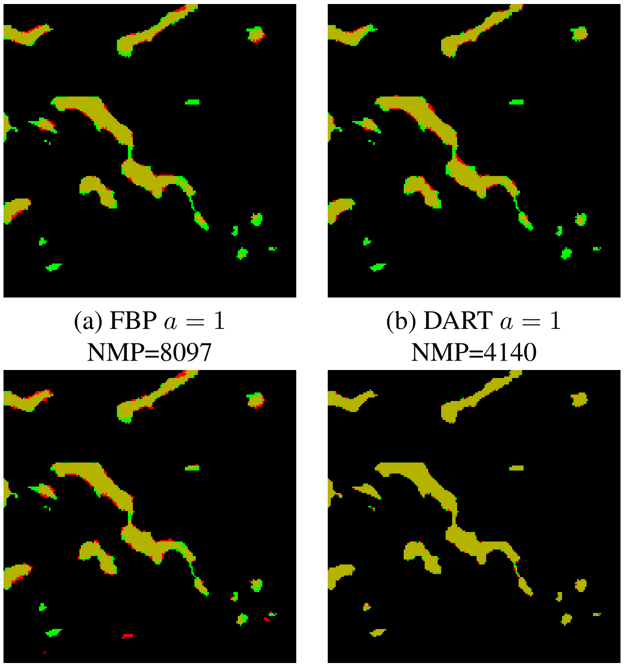

(a) FBP $a = 1$
NMP=8097

(b) DART $a = 1$
NMP=4140

(c) FBP $a = 8$
NMP=11149

(d) DART $a = 8$
NMP=627

Fig. 5. Thresholded FBP and DART reconstructions of Phantom B, for different levels of grid upsampling, and from only 36 projections with 256 radial samples.

The proposed technique is also applied on real X-ray CT data of trabecular bone of a rat, scanned at a 35μm resolution in a SkyScan 1076 μCT scanner. The resulting reconstructions are shown in Fig. 6. By visual inspection of two regions (denoted by a red and blue ellipse) in each of the 4 reconstructions, it can be seen that the upsampled DART image (Fig. 6(d)) more realistically recovers the small trabecular structures, whereas the trabeculae thicknesses in the red and blue regions of the FBP reconstructions are systematically under- and overestimated, respectively.

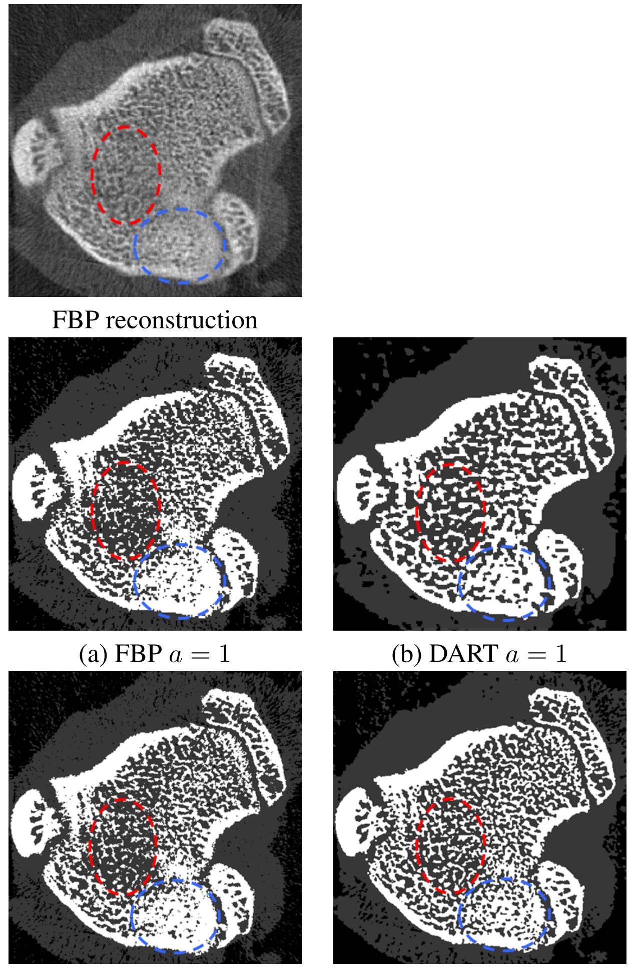

FBP reconstruction

(a) FBP $a = 1$

(b) DART $a = 1$

(c) FBP $a = 4$

(d) DART $a = 4$

Fig. 6. FBP and DART reconstructions of a rat trabecular bone slice close to the growing plate, from real X-ray CT data.

5. CONCLUSIONS

We proposed a method to enhance the effective spatial resolution of CT reconstructions without increasing the X-ray dose or scanning time. The method assumes that the object is composed of homogeneous materials. This prior knowledge is exploited by reconstructing the object on an upsampled grid using the discrete algebraic reconstruction technique DART. Experiments were run on simulated data as well as real X-ray CT data of the rat trabecular bone. Results show that the proposed method generates reconstructions with significantly more detail compared to conventional reconstruction algorithms.To quantify the results on real X-ray data, future work will consist of reconstructing 3D volumes of downsampled high resolution X-ray CT data and comparing the morphometric parameters from the low dose reconstructions with those of the high dose ground truth.

6. REFERENCES

[1] K.J. Batenburg and J. Sijbers, "DART: a fast heuristic algebraic reconstruction algorithm for discrete tomography," *Proc. of ICIP*, vol. 4, pp. 133–136, 2007.

[2] P.L. Salmon and A.Y. Sasov, *Chapter I-4 in Advanced Bioimaging Technologies in Assessment of the Quality of Bone and Scaffold Materials (Qin L. et al.)*, Springer Berlin Heidelberg, 2007.

[3] A.M. Parfitt et al., "Bone Histomorphometry: standardization of nomenclature, symbols and units," *J. Bone and Mineral Res.*, vol. 2, no. 6, pp. 595–610, 1987.